## ARTICLE  OPEN

Check for updates

# Biogenic silver nanoparticles-modified forward osmosis membranes with mitigated internal concentration polarization and enhanced antibacterial properties

Xing Wu[1,2], Fang Fang[1], Bifeng Zhang[1], Jun Jie Wu[3]✉ and Kaisong Zhang[1,4]✉

Thin-film composite forward osmosis (TFC-FO) membranes show the potential to be applied in water treatment applications. However, the TFC-FO membrane performance was limited by internal concentration polarization (ICP) and membrane fouling. In this study, a well-functioning TFC-FO membrane was produced by embedding biogenic silver nanoparticles (BioAg) into the polysulfone (PSf) substrate of a FO membrane. Effects of BioAg on membrane structure, filtration performance, antifouling, and antibacterial properties of the as-prepared FO membranes were examined. Results indicated that BioAg-modified FO membranes achieved improved surface hydrophilicity, higher porosity, and mitigated ICP, resulting in 2.5–4.4 times higher water flux than the pristine FO membranes. The BioAg-modified FO membrane also showed significantly improved antifouling and antibacterial ability. Moreover, the release velocity of silver nanoparticles in FO membranes was significantly slowed down by the construction of the polyamide layer. After 30 days of immersion in an aqueous solution, 96.5% of silver was retained in the optimized BioAg-modified FO membrane. The study offers an effective approach to simultaneously mitigate ICP and enhance the antifouling property of TFC-FO membranes through substrate modification.

*npj Clean Water* (2022)5:41 ; https://doi.org/10.1038/s41545-022-00190-1

## INTRODUCTION

The forward osmosis (FO) technology shows the potential to be used in desalination and wastewater treatment applications[1,2]. Currently, thin-film composite FO (TFC-FO) membranes enjoy popularity due to their advantages such as the superior water flux and rejection function in comparison to FO membranes fabricated by cellulose triacetate (CTA). However, TFC-FO membranes are still facing some hurdles, including the trade-off between water permeability and selectivity, the serious internal concentration polarization (ICP) phenomenon, and unneglected membrane fouling during the application[3,4].

Membrane modification by nanoparticles has been verified as an effective strategy to enhance membrane performance and properties. It was reported that nanoparticles such as silica nanoparticles[5], graphene oxides[6,7], MXene[8], and mixtures of nanoparticles[9,10] could be used as modifiers for membrane improvement. Among these nanoparticles, silver nanoparticles (AgNPs) showed excellent antibacterial performance and hydrophilicity, which have been successfully applied in membrane modification[11,12]. For example, Huang et al.[11] grafted chemical AgNPs on the surfaces of polysulfone (PSf) ultrafiltration membranes. The modified membrane witnessed a 35% increase in pure water permeability and an enhanced antibacterial property to *Escherichia coli* (*E. coli*) and *Bacillus subtilis* (*B. subtilis*). A similar result was observed in a study that grafts AgNPs on the surface of the thin film composite reverse osmosis membrane[12]. Although surface modification enables direct contact between antibacterial nanoparticles and feed solutions, which enhances the antibacterial performance of membranes, this method can result in a related high nanoparticle leaching if the adhesion between membrane surface and nanoparticles is not robust. Moreover, it

was reported in some studies that the water flux of FO membranes was slightly reduced after nanomaterials were coated on the surface of membranes[13]. In addition, surface modification hardly relieves the ICP phenomenon that happens inside the substrate of TFC-FO membrane. Therefore, another modification approach by embedding nanoparticles including carbon nanotubes[14] and titanium oxide[15] into the substrate of TFC-FO membranes was proposed and an alleviation of the ICP phenomenon has been reported. As a result of the mitigated ICP, water fluxes of these modified TFC-FO membranes were larger than those of pristine FO membranes. However, the poor distribution of nanoparticles at a high concentration in membranes is a critical issue that can negatively influence the performance of TFC-FO membranes[14]. For example, Zhang and co-authors reported that the addition of phosphorylated TiO$_2$ into polyvinylidene fluoride substrate effectively improved the porosity and reduced the ICP of FO membranes[16]. However, when the concentration of phosphorylated TiO$_2$ was higher than 0.3 wt%, the porosity of the substrate was reduced, and the performance of the as-prepared FO membrane was weakened due to the aggregation of phosphorylated TiO$_2$ in the substrate. Similar results were also observed in studies about silica[17], SiO$_2$-FMWNT[18], and LiCl[19].

Biogenic silver nanoparticles (BioAg) are prepared by reducing and capping silver ions using bacteria. The biosynthesis of AgNPs is an eco-friendly, cost-effective process, which has been regarded as "green nanotechnology"[20]. For BioAg, the bacteria were surrounded and attached by silver nanoparticles and functional groups such as hydroxide radical and carboxyl groups[21,22]. Such a structure could not only increase the hydrophilicity of BioAg but could also reduce the level of aggregation and silver leakage

[1]Key Laboratory of Urban Pollutant Conversion, Institute of Urban Environment, Chinese Academy of Sciences, Xiamen 361021, China. [2]CSIRO Manufacturing, Clayton South, Victoria 3169, Australia. [3]Department of Engineering, Durham University, Durham DH1 3LE, UK. [4]Key Lab of Marine Environment and Ecology, Ministry of Education, Ocean University of China, Qingdao 266100, China. ✉email: junjie.wu@durham.ac.uk; zhangkaisong@ouc.edu.cn
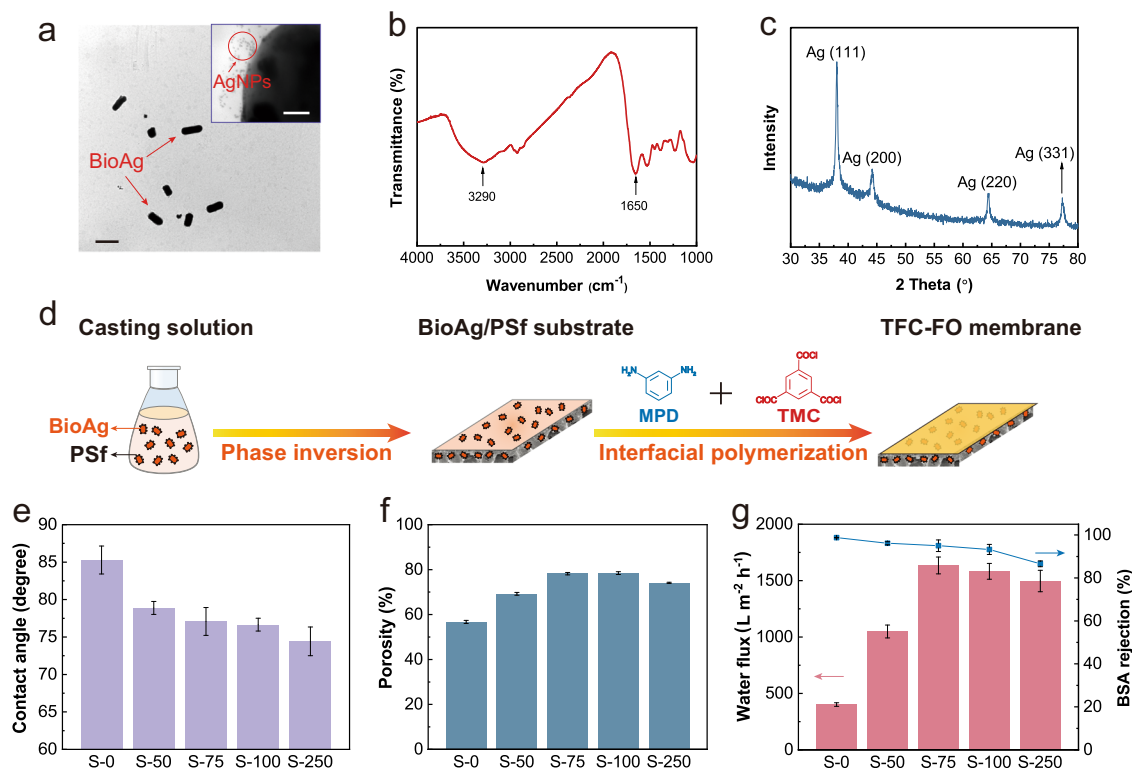
npj

**Fig. 1 BioAg and BioAg/PSf substrates. a** TEM image of BioAg particles (scale bar 2 μm), and a high-resolution TEM image of BioAg particles (inset, scale bar 100 nm). **b** FTIR of BioAg particles. **c** XRD of BioAg particles. **d** Schematic of the fabrication of the BioAg/PSf substrate and the BioAg modified TFC-FO membrane. **e** Contact angles of substrates containing different amounts of BioAg particles. **f** Porosity of substrates. **g** Pure water flux and BSA rejection of substrates. The error bars represent the standard deviations of the data.

compared with the traditional chemical silver nanoparticles[23–25]. Due to the advantages of BioAg, we considered that BioAg nanoparticles have a high potential to be used as modifiers to tune the properties of substrates for TFC-FO membranes and consequently mitigate the ICP of TFC-FO membranes. In addition, most previous studies on the antibacterial improvement of TFC membranes used the surface modification method, while few researchers investigated the antibacterial performance of TFC membranes when nanoparticles were embedded into membranes.

Herein, we reported an effective approach to concurrently enhance the permeability, mitigate ICP and boost the antibacterial properties of TFC-FO membranes by embedding BioAg into the PSf substrate before the construction of the polyamide layer via the interfacial polymerization process. The properties and performance of substrates were adjusted by tuning the concentration of BioAg and the impact of BioAg on the filtration performance, antifouling, and antibacterial properties of TFC-FO membranes were analyzed. This work demonstrates an effective method to produce effective TFC-FO membranes with weakened ICP and strong antibacterial properties.

## RESULTS AND DISCUSSION
### Effect of BioAg on substrates
The TEM image of BioAg (Fig. 1a and Supplementary Fig. 1) shows the uniform dispersion of BioAg. A high-resolution image (Fig. 1a inset) indicated that the AgNPs spread uniformly around the biomass or were embedded in the outer layers of the cell. Measured by the Nano Measurer software, the average diameter of AgNPs was $6.2 \pm 1.6$ nm. Figure 1b shows the FTIR spectra of BioAg. The peaks at 1650 and 3290 cm$^{-1}$ represent the C=O stretching of carbonyl content and hydroxyl groups respectively,

which indicated the hydrophilicity of BioAg[21]. Figure 1c displays the XRD result of BioAg. It could be observed that there were peaks at $2\theta = 38.03°$, 44.23°, 64.35°, and 77.29°, which could be indexed as (111), (200), (220), and (331) reflections of the face-centered cubic structure of metallic silver[22,26,27]. Figure 1d illustrates the fabrication process of BioAg-modified TFC-FO membranes. The BioAg were embedded into the PSf casting solution before the phase inversion process. Five types of PSf substrates with varied concentrations of BioAg were prepared and were named as S-0, S-50, S-75, S-100, and S-250, representing the concentration of BioAg in casting solution as 0.000, 0.050, 0.075, 0.100 and 0.250 wt% (Supplementary Table 1). After that, a series of TFC-FO membranes were fabricated based on these BioAg/PSf substrates. Based on the substrates that were used for fabrication (S-0 to S-250), these FO membranes were marked as F-0 to F-250, respectively.

Figure 1e reveals the influence of BioAg on the hydrophilicity of the substrate surfaces. The contact angles of the pristine S-0 substrate decreased from 85.3° to 74.4° in the S-250 membrane, demonstrating that the hydrophilicity of substrate membranes was enhanced after the introduction of hydrophilic BioAg[28]. In addition, with the increasing BioAg concentration from 0 to 0.100 wt%, the substrates exhibited higher porosity (Fig. 1f). Specifically, the S-100 membrane showed the largest porosity at 78.5%. The result proves that the inclusion of BioAg could affect the substrate morphology. This could be proven by SEM images, which will be discussed in more detail in the next section. However, the porosity of S-250 substrate (BioAg concentration = 0.250 wt%) experienced a slight decrease to 74.1%. The potential reason was the excess biomass of BioAg which blocked the membrane pores[22]. The pure water fluxes of substrates are exhibited in Fig. 1g. Compared with the pristine S-0 substrate, the S-75 and S-100 substrates showed 307% and 294%
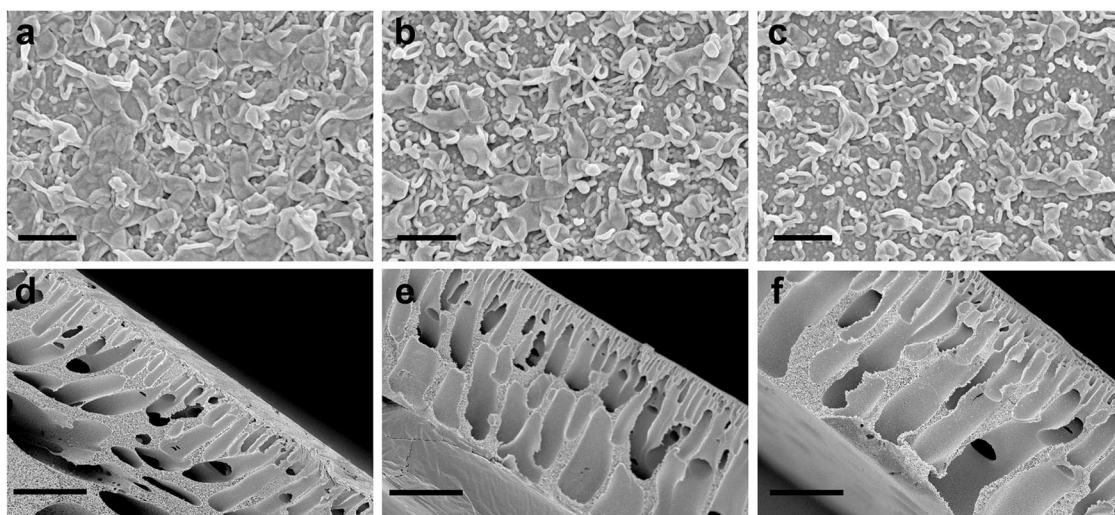
**Fig. 2 SEM images of BioAg-modified TFC-FO membranes.** The polyamide surfaces and the cross sections of the F-0 (**a, d**), F-75 (**b, e**), and F-250 membranes (**c, f**). The length of scale bars are 500 nm (**a–c**); 25 μm (**d–f**).
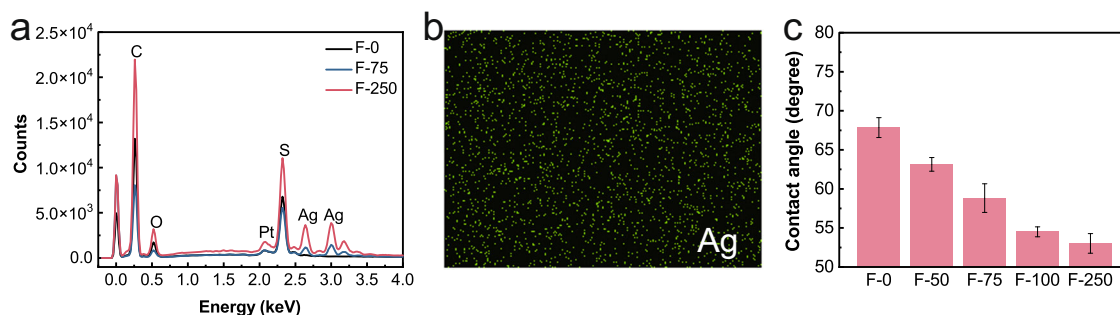


**Fig. 3 Characterization of BioAg-modified TFC-FO membranes. a** EDX spectrums of the F-0, F-75, and F-250 membranes. **b** EDX mapping of silver on the polyamide surface of the F-100 membrane. **c** Water contact angles of the polyamide surface of FO membranes. The error bars represent the standard deviations of the data.

increase in the pure water fluxes, respectively, although the BSA rejections were slightly reduced. The improved surface hydrophilicity and porosity of the substrates are major factors that directly caused the increase in water fluxes[29,30]. However, compared to the S-75 substrate, the water fluxes of S-100 and S-250 substrates dropped slightly even though their contact angles were lower. This was possibly the result of biomass blocking in the membrane pores at a high concentration of BioAg.

## Effects of BioAg on FO membranes

The SEM images of the surface and the cross-section of FO membranes (Fig. 2 and Supplementary Fig. 2) illustrate the typical "ridge and valley" structures of polyamide membranes[6]. It could be observed that more "nodular" structures were exposed without the cover of leaf-like structures, especially in the F-250 membrane. This result accords with previous work which revealed that the leaf-like structures on the surface of polyamide membranes were less when the substrate had higher hydrophilicity[31,32]. Figure 2 also shows the cross-sectional SEM images of the FO membranes. Although all FO membranes had finger-like porous structures and a sponge-like bottom section, the finger-like pores in the pristine F-0 membrane were narrow and short (Fig. 2d). The major reason for this was due to quick phase separation in the phase inversion process caused by the relatively lower casting solution viscosity[15]. As a result, finger-like pores were generated incompletely in a short time frame. In comparison, the viscosities of casting solutions with BioAg were higher[22,33], which reduced the diffusion

velocity of the solvent and offered more time to build finger-like pores. Moreover, the hydrophilic BioAg facilitated the transportation of water molecules into substrates, further improving the production of longer finger-like pores (Fig. 2e, f)[15].

Figure 3a shows the EDX spectrums of the pristine F-0 and BioAg-modified FO membranes. As the BioAg concentration increased, the peaks representing silver became more obvious. In addition, the silver elements on the polyamide surface of the F-100 membrane were distributed uniformly (Fig. 3b). The contact angle of water on the membrane surface decreased from 67.9° for the F-0 membrane to 53.0° for the F-250 membrane as the BioAg concentration increased (Fig. 3c). These results indicated that the AgNPs managed to embed in the FO membranes and could even be detected on the membrane surface. As a result, the hydrophilicity of the polyamide layer of the FO membranes improved, which could be attributed to the release of AgNPs from the substrates[34]. However, when the concentration of BioAg was 0.250 wt%, the distribution of silver elements was sightly ununiform (Supplementary Fig. 3), indicating the aggregation of BioAg at this concentration.

## Filtration performance of BioAg-modified FO membranes

The ICP is the major reason for the small water flux detected in FO membranes, which was related to the substrate structures[14,35]. Table 1 exhibits the water permeability (*A*), salt permeability (*B*), and structure parameter (*S*) of prepared FO membranes. It could be found that the *A* value increased while the concentration of

BioAg in FO membranes became larger, indicating the improved water permeability of prepared FO membranes by embedding BioAg. The major reasons for the improved water permeability were the increased porosity and hydrophilicity of FO membranes by the addition of BioAg[18,36]. In addition, the tuned substrate properties such as pore structure and surface hydrophilicity could also impact the thickness of the polyamide layer by influencing the interfacial polymerization process[32]. More specifically, due to the increased surface hydrophilicity, the S-100 substrate absorbed MPD molecules more easily, which decreased the diffusion rate of MPD molecules into the organic solvent to react with TMC molecules and consequently reduced the thickness of the polyamide layer in the F-100 membrane[37,38]. Using Nano Measurer software, the average thickness of the polyamide layer of the F-0 and F-100 membrane was calculated by measuring 60 different locations on cross-sectional SEM images shown in Supplementary Fig. 4. The average thickness of the polyamide layer in the F-100 membrane was 149.9 nm, which was significantly smaller than 270.1 nm for the F-0 membrane. The thinner polyamide layer provided a reduced distance of water transportation and increased water permeability. However, the increased salt permeability ($B$) indicated that the loading of BioAg has a negative impact on the selectivity of the polyamide layer. In

addition, the $S$ decreased from 2.07 mm for the F-0 membrane to 1.08 mm for the F-100 membrane, revealing the mitigated ICP of BioAg-modified FO membranes. However, the structure parameter ($S$) increased to 1.41 mm for the F-250 membranes when the BioAg concentration was 0.250 wt%. This was potentially due to the influence of BioAg on the properties of substrates including the finger-like structure and porosity. Moderate amounts (0.050–0.100 wt%) of BioAg can make the finger-like pores larger and increase substrate porosity, resulting in a more open structure of substrates[15,39,40]. Therefore, the ICP was mitigated. Inevitably, the $S$ value of the F-250 membrane was larger than that of the F-100 membrane, which was potentially due to the smaller porosity of S-250 caused by the aggregation of BioAg in the substrate when the concentration of BioAg was high (0.250 wt%)[22,41].

Figure 4a, b show the water fluxes and the specific salt fluxes ($J_s/J_w$) of the prepared FO membranes in the ALFS mode (the active layer facing the feed solution) and the ALDS mode (the active layer facing the draw solution), respectively. All BioAg-modified FO membranes exhibited higher water fluxes than that of the pristine F-0 membrane, indicating that the water fluxes of the FO membranes were improved by adding BioAg to the substrates. Specifically, contrasted with the pristine F-0 membrane, the water flux of the F-100 membrane showed 2.5 times and 4.4 times higher water fluxes in ALFS and ALDS mode, respectively. The major reasons for this improvement were the increased surface hydrophilicity, the mitigated ICP phenomenon, and the thinner polyamide layer in the F-100 membrane. Compared with the pristine F-0 membrane, BioAg-modified FO membranes had higher reverse solute fluxes in both the ALFS and the ALDS mode. However, the significantly improved water flux of BioAg-modified FO membranes resulted in smaller specific salt fluxes than that of the pristine F-0 membrane. The results exhibited that the embedding of BioAg in FO substrate can improve both the permeability and filtration efficiency of FO membranes.

**Table 1.** Properties of prepared FO membranes.

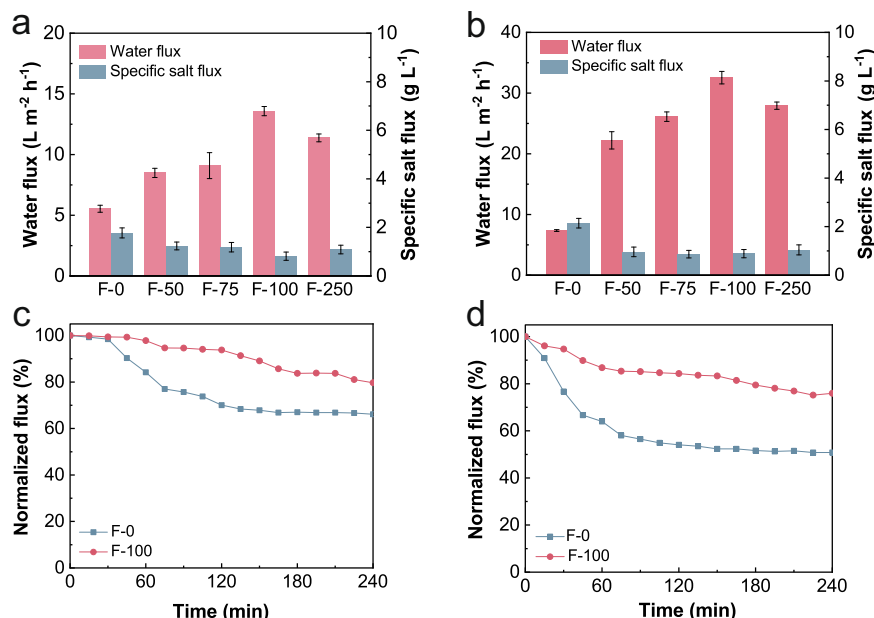| Membrane | Water permeability ($A$, L m$^{-2}$ h$^{-1}$ bar$^{-1}$) | Salt permeability ($B$, L m$^{-2}$ h$^{-1}$) | Structure parameter ($S$, mm) |
|---|---|---|---|
| F-0 | 0.51 ± 0.01 | 0.08 ± 0.01 | 2.07 |
| F-50 | 1.01 ± 0.02 | 0.15 ± 0.01 | 1.50 |
| F-75 | 1.30 ± 0.03 | 0.23 ± 0.01 | 1.50 |
| F-100 | 2.22 ± 0.01 | 0.38 ± 0.01 | 1.08 |
| F-250 | 2.69 ± 0.04 | 0.86 ± 0.02 | 1.41 |



**Fig. 4 Filtration performance of BioAg-modified TFC-FO membranes. a, b** Water flux and reverse solute flux of the prepared FO membranes in the ALFS mode and the ALDS mode, respectively (operating conditions: 2 mol L$^{-1}$ NaCl solution as the draw solution, 10 mmol L$^{-1}$ NaCl solution as the feed solution, cross-flow rate was 20 L h$^{-1}$). **c, d** Normalized flux of the F-0 and F-100 membranes in the ALFS mode and the ALDS mode, respectively (operating conditions: 2 mol L$^{-1}$ NaCl solution as the draw solution, 200 mg L$^{-1}$ BSA solution as the feed solution NaCl solution as the feed solution, cross-flow rate was 20 L h$^{-1}$). The error bars represent the standard deviations of the data.
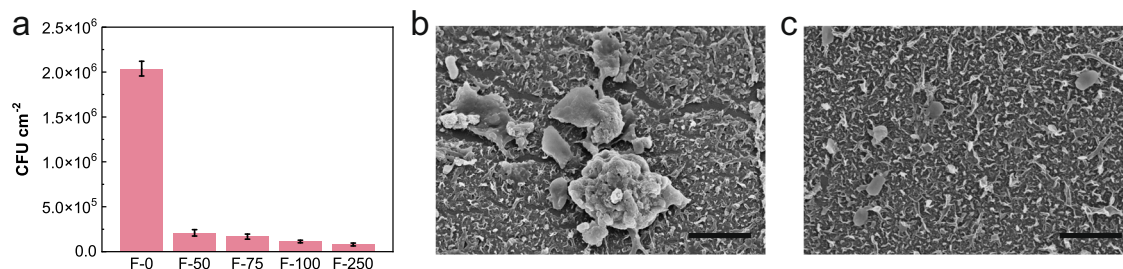
**Fig. 5 Antibacterial properties of BioAg-modified TFC-FO membranes. a** The amount of attached bacteria on the surface of prepared FO membranes. The error bars represent the standard deviations of the data. **b** SEM image of the polyamide surface of the fouled F-0 membrane (scale bar 2 μm). **c** SEM image of the polyamide surface of the fouled F-100 membrane (scale bar 2 μm).
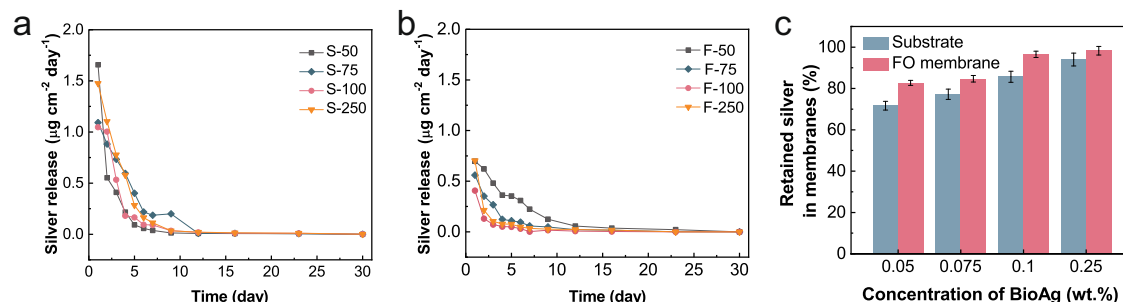


**Fig. 6 Silver retention in BioAg/PSf substrates and BioAg-modified TFC-FO membranes. a** Release of silver in the substrates. **b** Release of silver in the FO membranes. **c** The ratios of silver retention in substrates and FO membranes after 30-day immersion. The error bars represent the standard deviations of the data.

The antifouling property of the optimized BioAg-modified FO membrane (F-100) was evaluated by using 200 mg L$^{-1}$ of BSA aqueous solution as the feed solution (Fig. 4c, d). After 240-min continuous filtration, the water flux of the F-100 membrane dropped 24.7% and 31.7% in ALFS and ALDS mode, respectively. Compared with that, the pristine F-0 membrane witnessed larger water flux reductions with 35.8% (ALFS) and 60.9% (ALDS). However, it should be mentioned that the initial water flux of the F-100 membrane in the ALDS mode was 2.4 times higher than that of the F-100 membrane in the ALFS mode. What contributed to the improved antifouling property of the F-100 membrane was mainly the increased surface hydrophilicity of BioAg-modified FO membranes. A hydrophilic membrane showed a mitigated fouling tendency because it hindered the attachment of foulants on the surface of membranes[42–45]. Moreover, compared with the membranes in the ALFS mode, all membranes in the ALDS mode showed a more obvious water flux reduction caused by severer membrane fouling in the ALDS mode. When FO membranes were filtrated in the ALDS mode, foulants would be introduced into the pores of substrates and formed a cake layer. The solute concentrations near the membrane surfaces would increase, which was noted as cake-enhanced concentration polarization (CE-CP), causing a stronger concentration polarization phenomenon and a significant drop in water fluxes[42]. Therefore, the smaller reduction of water flux for the F-100 membrane also indicated a strengthened property of the membrane to lessen the influences of CE-CP. However, a further comprehensive investigation should be conducted to understand the fouling mechanism and the impact of fouling on the selectivity of FO membranes.

## Antibacterial properties of BioAg-modified FO membranes

*P. aeruginosa* is a microorganism present in water, which can cause pneumonia and other infections[46]. In this study, *P. aeruginosa* was selected as the model bacterial for the antibacterial properties test. The antibacterial property of membranes was evaluated by counting the bacteria on the fouled membranes

after the 6-h continuous filtration of the feed solution which contained *P. aeruginosa*. Figure 5a exhibited the amount of attached bacteria on the surface of prepared FO membranes with different BioAg loadings. BioAg-modified FO membranes had much fewer bacteria attached on the surface of membranes. Moreover, the CFU value of membranes decreased as the BioAg in membranes increased. When the concentration of BioAg was larger than 0.050 wt%, the BioAg-modified FO membranes showed more than 90% reduction in the CFU value compared to the pristine F-0 membrane. The antibacterial activity was due to the presence of AgNPs on the surface of FO membranes which was verified by EDX results. The AgNPs could interact with the proteins and the enzymes on the surfaces of bacterial cells and hence could influence the stability of cells and their DNA replication. Therefore, the growth of bacterial cells was hindered and the biofouling of membranes decreased[6,47,48]. Figure 5b, c show the SEM images of polyamide surfaces of the fouled F-0 and F-100 membranes. It could be found that on the surface of the F-0 membrane, besides *P. aeruginosa* bacteria, there were extracellular polymeric substances (EPS) produced by *P. aeruginosa* bacteria. EPS could provide nutrients for bacteria and could facilitate the attachment of bacteria, leading to more serious biofouling[49]. Compared with the F-0 membrane, the surface of the F-100 membrane was cleaner. This result was associated with the enhanced antibacterial properties and the improved hydrophilic surface of BioAg-modified FO membranes, which synergistically reduced the growth and attachment of bacteria on the surface of FO membranes and moderated the biofouling of membranes.

To investigate whether the velocity of silver leaching was influenced by the formation of polyamide layers in FO membranes, the silver leaching of both the substrates and the FO membranes was tested by ICP-MS over 30 days. Results indicated that the speed of silver leaching in both substrates and FO membranes decreased as time went by (Fig. 6a, b). All membranes released relatively large amounts of silver in the first 10 days, while the releasing rate dropped and stayed at a low level near zero after the 10th day. Compared with the substrate membranes, the

**Table 2.** Comparison of FO filtration performances.

| Substrate | Additives | Feed solution | Draw solution | Water flux ($L\,m^{-2}\,h^{-1}$) | Increase in water flux | Specific salt flux ($g\,L^{-1}$) | Reference |
|---|---|---|---|---|---|---|---|
| PSf | Pristine FO | 10 mM NaCl | 2 M NaCl | 5.5 (ALFS)<br>7.4 (ALDS) | 147% (ALFS)<br>339% (ALDS) | 1.8 (ALFS)<br>2.1 (ALDS) | This work |
| | BioAg-0.1 wt% | | | 13.6 (ALFS)<br>32.5 (ALDS) | | 0.8 (ALFS)<br>0.8 (ALDS) | |
| CTA | Pristine FO | 10 mM NaCl | 1 M NaCl | 8.7 (ALFS)<br>9.1 (ALDS) | 79% (ALFS)<br>76% (ALDS) | 0.17 (ALFS) | [50] |
| | CNF-0.5 wt% | | | 15.6 (ALFS)<br>16.0 (ALDS) | | 0.06 (ALFS) | |
| PES | Pristine FO | DI water | 2 M NaCl | 16.5 (ALFS)<br>22.4 (ALDS) | 75% (ALFS)<br>70% (ALDS) | 0.4 (ALFS)<br>0.5 (ALDS) | [51] |
| | Fe$_3$O$_4$-0.2 wt% | | | 28.8 (ALFS)<br>38.1 (ALDS) | | 0.5 (ALFS)<br>0.5 (ALDS) | |
| PSf | Pristine FO | DI water | 2 M NaCl | 3.6 (ALFS)<br>5.5 (ALDS) | 372% (ALFS)<br>401% (ALDS) | 2.6 (ALFS)<br>3.0 (ALDS) | [62] |
| | CaCO$_3$-5.0 wt% | | | 17.0 (ALFS)<br>27.6 (ALDS) | | 1.7 (ALFS)<br>2.6 (ALDS) | |
| PSf | Pristine FO | DI water | 0.6 M NaCl | 3.6 (ALFS)<br>5.1 (ALDS) | 92% (ALFS)<br>110% (ALDS) | 1.5 (ALFS)<br>1.3 (ALDS) | [52] |
| | LiCl-3 wt% | | | 6.9 (ALFS)<br>10.7 (ALDS) | | 1.0 (ALFS)<br>0.8 (ALDS) | |
| PES | Pristine FO | DI water | 0.6 M NaCl | 7.0 (ALFS) | 71% (ALFS) | 0.8 (ALFS) | [53] |
| | Acid functionalized CNTs-0.5 wt% | | | 12.0 (ALFS) | | 0.6 (ALFS) | |
| PSf | Pristine FO | DI water | 1 M NaCl | 8.6 (ALFS)<br>15.3 (ALDS) | 8% (ALFS)<br>46% (ALDS) | 0.8 (ALFS)<br>0.5 (ALDS) | [54] |
| | Layered double hydroxide/GO-2 wt% | | | 9.3 (ALFS)<br>22.3 (ALDS) | | 0.7 (ALFS)<br>0.5 (ALDS) | |

FO membranes showed smaller amounts of released silver from the beginning. Figure 6c shows the silver retention ratios in substrates and FO membranes by comparing the silver amount in membranes before and after the 30-day immersion test. All ratios associated with the substrates ranged from 71.7% to 94.0%, indicating large amounts of silver remained in the substrate membranes after 30 days of immersion. Additionally, compared with the ratios of the substrate membranes, the silver retention ratios of the FO membranes were higher (ranging from 84.7% to 98.3%), which indicated that after the construction of the polyamide layer, the speed of silver release from substrates was decreased. The potential reason was due to smaller pores in the polyamide layer, which reduced the release speed of silver. Therefore, the BioAg-modified FO membrane showed the potential to possess a long-term antibacterial property. However, for more in-depth investigation, further studies about the testing of the silver leaching speed in BioAg-modified FO membranes could be conducted in the FO filtration system. Table 2 presents the FO filtration performance of BioAg-modified membranes and other FO membranes based on nanomaterial-incorporated substrates. The results indicated that the addition of BioAg effectively improved the water flux of FO membranes by 147% and 339% in the ALFS and the ALDS mode, respectively, which were higher than some other types of nanomaterials[50–54]. It should be mentioned that besides the improved FO filtration performance, the addition of BioAg also enhanced the antibacterial properties, which has rarely been reported for other FO membranes based on nanomaterials-incorporated substrates.

The study shows the utilization of BioAg to prepare TFC-FO membranes with enhanced filtration performance, mitigated ICP, and improved antibacterial properties. Results indicated that the surface hydrophilicity, porosity, and water permeability of PSf substrates were enhanced by the addition of BioAg into casting solutions. By optimizing the amount of BioAg in PSf substrates, the improved FO membrane exhibited 2.7–4.4 times higher water fluxes than the pristine FO membrane without a sacrifice of selectivity due to the better hydrophilicity and the mitigated ICP phenomenon of the FO membranes. Besides, BioAg-modified FO membranes performed well in hindering the organic fouling and reducing the growth of *P. aeruginosa*. The construction of the polyamide layer effectively reduced the release of silver from substrates, suggesting the potential long-term antibacterial properties of BioAg-modified TFC-FO membranes. This study sheds light on the fabrication of well-functioning and antibacterial TFC-FO membranes by embedding nanoparticles into substrates. Further studies to explain the process of silver release from the substrate to the surface of BioAg-modified FO membrane can be valuable. Moreover, the application of real wastewater and a long-term continuous filtration process can be conducted to further evaluate the practical feasibility of the BioAg-modified FO membrane for wastewater treatment.

## METHODS
### Materials and chemicals
Polysulfone (PSf, Solvay P3500, BASF Co., China), polyvinylpyrrolidone (PVP K30, Sigma Aldrich Ltd., China), and 1-methyl-2-pyrrolidinone (NMP, ≥99%, Sinopharm Chemical Reagent Co., Ltd., China) were used for the PSf substrate membrane preparation. Trimesoyl chloride (TMC, Aladdin, China), m-phenylenediamine (MPD, Aladdin, China), and n-hexane (99%, Sinopharm Chemical Reagent Co., Ltd., China) were used for the TFC-FO membrane preparation. Sodium chloride (NaCl, Sinopharm Chemical Reagent Co., Ltd., China) and bovine serum albumin (BSA, 69 KDa, Solarbio Science & Technology Co., Ltd., China) was applied for membrane performance testing. Phosphate buffer saline (PBS, including

1.093 g Na$_2$HPO$_4$, 0.276 g NaH$_2$PO$_4$, and 8.475 g NaCl in 1 L deionized (DI) water was used to keep bacteria in a normal physiological state.

## Synthesis of BioAg and BioAg-modified FO membranes

BioAg nanoparticles were synthesized by reducing silver ions using *Lactobacillus fermentum LMG 8900* according to the method from the previous studies[21,22,55]. Briefly, 10 g of dried *L.fermentum* biomass was suspended in 1 L of Milli-Q water. After that 10 g of diamine silver and 0.2 mol of NaOH were added to the solution. After 24 h of incubation at 30 °C, the solution was centrifuged and washed with Milli-Q water and the precipitated BioAg was dried by freezing-drying.

The BioAg/PSf substrates were fabricated by the phase inversion process. To prepare 100 g of casting solution, different amounts of dry BioAg powder were mixed with 20 g of NMP in 30 min of ultra-sonication, while 0.5 g PVP and 17.5 g PSf were disposed into the rest of the NMP solution and were stirred at 60 °C over-night. The homogenous PSf solutions were mixed with the BioAg solutions in a stirring condition. The casting solution was poured on a clean glass plate and the membrane was cast by a casting knife (height = 175 μm). Afterward, the glass plate was immersed in a deionized (DI) water bath at once. After peeling off, the membrane was stored in DI water for further utilization. Five types of PSf substrates with varied concentrations of BioAg were prepared and were named S-0, S-50, S-75, S-100, and S-250, representing the concentration of BioAg in casting solution as 0.000, 0.050, 0.075, 0.100, and 0.250 wt% (Supplementary Table 1).

The polyamide layers of the FO membranes were fabricated through the typical interfacial polymerization process. Generally, the substrate was soaked in the 2.0 wt% MPD aqueous solutions for 2 min. After the excess MPD solutions were drained, the substrate membrane was soaked in the organic phase (0.1 wt% TMC in *n*-hexane). After 1 min, TMC was removed and the membrane was dried in an oven at 60 °C for 8 min. Based on the substrates that were used for fabrication (S-0 to S-250), these FO membranes were marked as F-0 to F-250, respectively.

## Characterization of BioAg and membranes

The morphology of BioAg was observed by transmission electron microscopy (TEM, HITACHI H-7650). The Nano Measurer software was used to calculate the size of AgNPs around BioAg. The functional groups around BioAg were studied using a Fourier-transform infrared spectroscope (FTIR, Nicolet iS10, Thermo Fisher Scientific) with a range from 500 to 4000 cm$^{-1}$. X-ray diffraction (XRD) of BioAg was investigated using the X-ray diffraction meter (X'Pert PRO, PANalytical B.V.) with 2$\theta$ ranging from 30° to 80°. The contact angles of the membranes were tested using the sessile drop analysis system (DSA100, KRUSS). The contact angle value of each sample shown in this study was the average value from five randomly chosen spots in each sample after 1 s of contact between the water droplet and the membrane surface. In addition, the morphological structures of FO membranes were studied by a field emission scanning electron microscope (FESEM, HITACHI S-4800). Moreover, an energy dispersive X-ray spectra (EDX) system was applied to detect the existence of silver elements on the surface of the FO membranes.

## Performance evaluation of FO membranes

The properties of BioAg/PSf substrates including porosity, pure water flux, and BSA rejection were tested according to the previous studies[56]. Detailed descriptions of methods can be found in the Supplementary Methods. A cross-flow reverse osmosis filtration system was used to examine the water permeability coefficient (*A*) and the salt permeability coefficient (*B*) of prepared FO membranes by using 10 L DI water and 10 L NaCl aqueous solution (20 mmol L$^{-1}$) as the feed solution, respectively[15,57]. The

effective membrane area was 33.8 cm$^2$ and the operation pressure was kept at 2 bar. The membrane flux (*J*) and *A* were calculated by equations below:

$$J = \frac{\Delta V}{A_m \times t} \tag{1}$$

$$A = \frac{J}{\Delta P} \tag{2}$$

where $\Delta V$ (L) represents the permeated water volume during the permeation time *t* (h), $A_m$ (m$^2$) represents the membrane area and $\Delta P$ (bar) is the operation pressure difference.

The salt rejection (*R*) and salt permeability coefficient (*B*) were calculated by Eqs. (3) and (4), respectively:

$$R = \left(1 - \frac{C_p}{C_f}\right) \times 100 \tag{3}$$

$$\frac{1-R}{R} = \frac{B}{A \times (\Delta P - \Delta \pi)} \tag{4}$$

where $C_p$ (g L$^{-1}$) and $C_f$ (g L$^{-1}$) are the NaCl concentrations of the permeate solution and the feed solution, respectively, and $\Delta \pi$ (bar) is the difference in osmosis pressures across the membrane.

All FO membranes with an effective membrane area of 33.8 cm$^2$ were tested in a cross-flow FO filtration system in both the ALFS mode (the active layer facing the feed solution) and the ALDS mode (the active layer facing the draw solution) under room temperature with a cross-flow rate at 20 L h$^{-1}$ [15,58]. Each type of FO membrane was tested in triplicate to minimize experimental errors. 2 L of NaCl solution (2 mol L$^{-1}$) was applied as the draw solution, and 2 L of 10 mmol L$^{-1}$ NaCl solution was used as the feed solution according to the previous studies[59]. A digital weight balance and a conductivity meter were applied to monitor the variation of the weight of the draw solution and the conductivity of the feed solution, respectively. After 30 min of filtration, the membrane reached a steady state, and then the water flux ($J_w$) and the reverse solute flux ($J_s$) were checked every 15 min for at least 5 times to calculate the average values. $J_w$ and $J_s$ could be achieved by the following equations:

$$J_w = \frac{\Delta V}{A_m \times t} \tag{5}$$

$$J_s = \frac{C_t \times V_t - C_0 \times V_0}{A_m \times t} \tag{6}$$

where $C_0$ (g L$^{-1}$) and $C_t$ (g L$^{-1}$) are the initial and final concentrations of NaCl in the feed solution, respectively. $V_0$ (L) and $V_t$ (L) represent the initial and final volume of feed solution, respectively.

The structure parameter (*S*) of FO membranes was tested in ALFS mode by Eq. (7) according to the classical ICP model[15,60]:

$$S = \frac{D}{J_w}\left[\ln\frac{A\pi_{draw} + B}{A\pi_{feed} + J_w + B}\right] \tag{7}$$

where $\pi_{draw}$ (bar) and $\pi_{feed}$ (bar) represent the osmotic pressure of the draw solution and the feed solution, respectively, and *D* (m$^2$ s$^{-1}$) is the solution diffusion coefficient.

## Evaluation of antifouling and antibacterial properties

To reveal the improved effects of BioAg on the antifouling property of prepared FO membranes against organic foulant, 2 L of 200 mg L$^{-1}$ BSA aqueous solution was selected as the feed solution while 2 L of 2 mol L$^{-1}$ NaCl aqueous solution acted as the draw solution[61]. This experiment was operated for 240 min at room temperature. Moreover, the antibacterial property of FO membranes was investigated by a biofouling experiment. Before the experiment, the FO filtration system was successively cleaned and disinfected with 0.5% NaClO, EDTA (5 mmol L$^{-1}$), and 95% ethanol. Each of the

above solutions (2 L) was circulated through the system for 1 h. After that, the FO system was cleared by DI water three times. To run the biofouling experiment, a FO membrane was placed into the FO filtration system. 2 L NaCl aqueous solution (0.9 wt%) containing $(17.1 \pm 0.8) \times 10^9$ cells $L^{-1}$ of *P.aeruginosa* and 2 L of NaCl solution $(2 \, mol \, L^{-1})$ were used as the feed solution and the draw solution respectively. Each FO membrane was tested for 6 h.

After the biofouling experiment, the bacteria attached to the surface of FO membranes were characterized by the colony-forming unit (CFU) and SEM test. Circular samples with a diameter of 6 mm were cut from two different fouled areas of each membrane and were then transferred to 10 mL saline solution, respectively. After 15 min of sonication, the collected solution was sequentially diluted 10-fold in saline solution. The diluted solution was then spread on LB agar plates. Before counting the CFU, the LB agar plates were kept overnight at 37 °C. Each sample was tested in duplicate. In addition, the morphology of fouled membranes was characterized by SEM. To fix the foulants on membrane surfaces, fouled membranes were immersed in 2.5% glutaraldehyde in $0.1 \, mol \, L^{-1}$ PBS for 2 h and were then dehydrated by 30%, 50%, 70%, 90%, 100% ethanol for 15 min. After being dried, membranes were sputter-coated with platinum, followed by an SEM test.

The velocity of silver leaching of both substrates and FO membranes was tested under an immersion experiment. Firstly, both samples of the substrate membranes and the FO membranes were cut into 9 cm$^2$ and stored in 30 mL nitric acid solution. After 3 days of shaking, the membranes were broken, and then the nitric acid solution was diluted and tested by an inductively coupled plasma mass spectrometry (ICP-MS, Agilent, model 7500CX) to calculate the total silver amount in membranes. Additionally, to measure the amount of released silver, other membrane samples with 9 cm$^2$ were also immersed in 30 mL Milli-Q water. After a specific time, the membranes were taken out and immersed in additional Milli-Q water, while the former Mill-Q water was tested by ICM–MS to measure the amount of silver. This experiment was operated for 30 days.

## DATA AVAILABILITY

Data generated during and/or analyzed during this study are available from the corresponding author on reasonable request.

## REFERENCES

1. Chung, T.-S. et al. Emerging forward osmosis (FO) technologies and challenges ahead for clean water and clean energy applications. *Curr. Opin. Chem. Eng.* **1**, 246–257 (2012).
2. Wu, X., Lau, C. H., Pramanik, B. K., Zhang, J. & Xie, Z. State-of-the-art and opportunities for forward osmosis in sewage concentration and wastewater treatment. *Membranes* **11**, 305 (2021).
3. Zhu, Y. et al. Single-walled carbon nanotube film supported nanofiltration membrane with a nearly 10 nm thick polyamide selective layer for high-flux and high-rejection desalination. *Small* **12**, 5034–5041 (2016).
4. Gao, S. et al. Ultrathin polyamide nanofiltration membrane fabricated on brush-painted single-walled carbon nanotube network support for ion sieving. *ACS Nano* **13**, 5278–5290 (2019).
5. Niksefat, N., Jahanshahi, M. & Rahimpour, A. The effect of SiO2 nanoparticles on morphology and performance of thin film composite membranes for forward osmosis application. *Desalination* **343**, 140–146 (2014).
6. Chae, H.-R., Lee, J., Lee, C.-H., Kim, I.-C. & Park, P.-K. Graphene oxide-embedded thin-film composite reverse osmosis membrane with high flux, anti-biofouling, and chlorine resistance. *J. Membr. Sci.* **483**, 128–135 (2015).
7. Wu, X., Tanner, J., Ng, D., Acharya, D. & Xie, Z. Sewage concentration via a graphene oxide modified thin-film nanocomposite forward osmosis membrane: enhanced performance and mitigated fouling. *Chem. Eng. J.* **420**, 127718 (2021).
8. Wu, X. et al. Production of cooling water by Ti3C2Tx MXene interlayered forward osmosis membranes for post-combustion CO2 capture system. *J. Membr. Sci.* **641**, 119877 (2022).
9. Safarpour, M., Khataee, A. & Vatanpour, V. Thin film nanocomposite reverse osmosis membrane modified by reduced graphene oxide/TiO2 with improved desalination performance. *J. Membr. Sci.* **489**, 43–54 (2015).
10. Ghanbari, M. et al. Super hydrophilic TiO2/HNT nanocomposites as a new approach for fabrication of high performance thin film nanocomposite membranes for FO application. *Desalination* **371**, 104–114 (2015).
11. Huang, L. et al. In situ immobilization of silver nanoparticles for improving permeability, antifouling and anti-bacterial properties of ultrafiltration membrane. *J. Membr. Sci.* **499**, 269–281 (2016).
12. Yin, J., Yang, Y., Hu, Z. & Deng, B. Attachment of silver nanoparticles (AgNPs) onto thin-film composite (TFC) membranes through covalent bonding to reduce membrane biofouling. *J. Membr. Sci.* **441**, 73–82 (2013).
13. Akther, N., Ali, S. M., Phuntsho, S. & Shon, H. Surface modification of thin-film composite forward osmosis membranes with polyvinyl alcohol–graphene oxide composite hydrogels for antifouling properties. *Desalination* **491**, 114591 (2020).
14. Wang, Y., Ou, R., Ge, Q., Wang, H. & Xu, T. Preparation of polyethersulfone/carbon nanotube substrate for high-performance forward osmosis membrane. *Desalination* **330**, 70–78 (2013).
15. Emadzadeh, D., Lau, W. J., Matsuura, T., Ismail, A. F. & Rahbari-Sisakht, M. Synthesis and characterization of thin film nanocomposite forward osmosis membrane with hydrophilic nanocomposite support to reduce internal concentration polarization. *J. Membr. Sci.* **449**, 74–85 (2014).
16. Zhang, X. et al. Confining migration of amine monomer during interfacial polymerization for constructing thin-film composite forward osmosis membrane with low fouling propensity. *Chem. Eng. Sci.* **207**, 54–68 (2019).
17. Liu, X. & Ng, H. Y. Fabrication of layered silica–polysulfone mixed matrix substrate membrane for enhancing performance of thin-film composite forward osmosis membrane. *J. Membr. Sci.* **481**, 148–163 (2015).
18. Zhang, X. et al. Construction of SiO2@ MWNTs incorporated PVDF substrate for reducing internal concentration polarization in forward osmosis. *J. Membr. Sci.* **564**, 328–341 (2018).
19. Ma, N. et al. Nanocomposite substrates for controlling internal concentration polarization in forward osmosis membranes. *J. Membr. Sci.* **441**, 54–62 (2013).
20. Rai, M. et al. Biogenic silver nanoparticles: what we know and what do we need to know? *Nanomaterials* **11**, 2901 (2021).
21. Zhang, M., Zhang, K., De Gusseme, B. & Verstraete, W. Biogenic silver nanoparticles (bio-Ag 0) decrease biofouling of bio-Ag 0/PES nanocomposite membranes. *Water Res.* **46**, 2077–2087 (2012).
22. Zhang, M., Field, R. W. & Zhang, K. Biogenic silver nanocomposite polyethersulfone UF membranes with antifouling properties. *J. Membr. Sci.* **471**, 274–284 (2014).
23. Sintubin, L. et al. Lactic acid bacteria as reducing and capping agent for the fast and efficient production of silver nanoparticles. *Appl. Microbiol. Biotechnol.* **84**, 741–749 (2009).
24. Song, J. Y. & Kim, B. S. Rapid biological synthesis of silver nanoparticles using plant leaf extracts. *Bioprocess. Biosyst. Eng.* **32**, 79–84 (2009).
25. Gurunathan, S. et al. Multidimensional effects of biologically synthesized silver nanoparticles in *Helicobacter pylori*, *Helicobacter felis*, and human lung (L132) and lung carcinoma A549 cells. *Nanoscale Res. Lett.* **10**, 1–17 (2015).
26. Lee, J. H., Kang, S., Lee, J. Y. & Jung, J. H. A tetrazole-based metallogel induced with Ag+ ion and its silver nanoparticle in catalysis. *Soft Matter* **8**, 6557–6563 (2012).
27. Sadeghi, B., Rostami, A. & Momeni, S. Facile green synthesis of silver nanoparticles using seed aqueous extract of *Pistacia atlantica* and its antibacterial activity. *Spectrochim. Acta Part A: Mol. Biomol. Spectrosc.* **134**, 326–332 (2015).
28. Zhang, J. et al. Synergetic effects of oxidized carbon nanotubes and graphene oxide on fouling control and anti-fouling mechanism of polyvinylidene fluoride ultrafiltration membranes. *J. Membr. Sci.* **448**, 81–92 (2013).
29. Ayyaru, S. & Ahn, Y.-H. Application of sulfonic acid group functionalized graphene oxide to improve hydrophilicity, permeability, and antifouling of PVDF nanocomposite ultrafiltration membranes. *J. Membr. Sci.* **525**, 210–219 (2017).
30. Li, S., Cui, Z., Zhang, L., He, B. & Li, J. The effect of sulfonated polysulfone on the compatibility and structure of polyethersulfone-based blend membranes. *J. Membr. Sci.* **513**, 1–11 (2016).
31. Zhou, Z., Lee, J. Y. & Chung, T.-S. Thin film composite forward-osmosis membranes with enhanced internal osmotic pressure for internal concentration polarization reduction. *Chem. Eng. J.* **249**, 236–245 (2014).
32. Wu, X., Kohl, T. M., Tsanaktsidis, J. & Xie, Z. Improved performance and mitigated internal concentration polarization of thin-film composite forward osmosis membrane with polysulfone/polyaniline substrate. *ACS Appl. Polym. Mater.* **3**, 5758–5766 (2021).

33. Huang, J., Arthanareeswaran, G. & Zhang, K. Effect of silver loaded sodium zirconium phosphate (nanoAgZ) nanoparticles incorporation on PES membrane performance. *Desalination* **285**, 100–107 (2012).

34. Pan, S. –F. et al. Synthesis of silver nanoparticles embedded electrospun PAN nanofiber thin-film composite forward osmosis membrane to enhance performance and antimicrobial activity. *Ind. Eng. Chem. Res.* **58**, 984–993 (2018).

35. Wang, Y., Ou, R., Wang, H. & Xu, T. Graphene oxide modified graphitic carbon nitride as a modifier for thin film composite forward osmosis membrane. *J. Membr. Sci.* **475**, 281–289 (2015).

36. Pan, Y.-H., Zhao, Q.-Y., Gu, L. & Wu, Q.-Y. Thin film nanocomposite membranes based on imologite nanotubes blended substrates for forward osmosis desalination. *Desalination* **421**, 160–168 (2017).

37. Park, S.-J. et al. A facile and scalable fabrication method for thin film composite reverse osmosis membranes: dual-layer slot coating. *J. Mater. Chem. A* **5**, 6648–6655 (2017).

38. Zarshenas, K., Jiang, G., Zhang, J., Jauhar, M. A. & Chen, Z. Atomic scale manipulation of sublayer with functional TiO2 nanofilm toward high-performance reverse osmosis membrane. *Desalination* **480**, 114342 (2020).

39. Tiraferri, A., Yip, N. Y., Phillip, W. A., Schiffman, J. D. & Elimelech, M. Relating performance of thin-film forward osmosis membranes to support layer formation and structure. *J. Membr. Sci.* **367**, 340–352 (2011).

40. Lay, W. C. et al. Factors affecting flux performance of forward osmosis systems. *J. Membr. Sci.* **394**, 151–168 (2012).

41. Rastgar, M., Shakeri, A., Bozorg, A., Salehi, H. & Saadattalab, V. Impact of nanoparticles surface characteristics on pore structure and performance of forward osmosis membranes. *Desalination* **421**, 179–189 (2017).

42. She, Q., Wang, R., Fane, A. G. & Tang, C. Y. Membrane fouling in osmotically driven membrane processes: a review. *J. Membr. Sci.* **499**, 201–233 (2016).

43. Zhu, X. & Elimelech, M. Colloidal fouling of reverse osmosis membranes: measurements and fouling mechanisms. *Environ. Sci. Technol.* **31**, 3654–3662 (1997).

44. Mi, B. & Elimelech, M. Organic fouling of forward osmosis membranes: fouling reversibility and cleaning without chemical reagents. *J. Membr. Sci.* **348**, 337–345 (2010).

45. Vrijenhoek, E. M., Hong, S. & Elimelech, M. Influence of membrane surface properties on initial rate of colloidal fouling of reverse osmosis and nanofiltration membranes. *J. Membr. Sci.* **188**, 115–128 (2001).

46. Bauman, S. J. & Kuehn, M. J. Purification of outer membrane vesicles from *Pseudomonas aeruginosa* and their activation of an IL-8 response. *Microb. Infect.* **8**, 2400–2408 (2006).

47. Kora, A. J. & Arunachalam, J. Assessment of antibacterial activity of silver nanoparticles on *Pseudomonas aeruginosa* and its mechanism of action. *World J. Microbiol. Biotechnol.* **27**, 1209–1216 (2011).

48. Marambio-Jones, C. & Hoek, E. M. A review of the antibacterial effects of silver nanomaterials and potential implications for human health and the environment. *J. Nanopart. Res.* **12**, 1531–1551 (2010).

49. Nguyen, T., Roddick, F. A. & Fan, L. Biofouling of water treatment membranes: a review of the underlying causes, monitoring techniques and control measures. *Membranes* **2**, 804–840 (2012).

50. Dabaghian, Z. & Rahimpour, A. Carboxylated carbon nanofibers as hydrophilic porous material to modification of cellulosic membranes for forward osmosis desalination. *Chem. Eng. Res. Des.* **104**, 647–657 (2015).

51. Darabi, R. R., Peyravi, M., Jahanshahi, M. & Qhoreyshi Amiri, A. A. Decreasing ICP of forward osmosis (TFN-FO) membrane through modifying PES-Fe3O4 nanocomposite substrate. *Korean J. Chem. Eng.* **34**, 2311–2324 (2017).

52. Darwish, N. B. et al. Effect of lithium chloride additive on forward osmosis membranes performance. *J. Water Process Eng.* **33**, 101049 (2020).

53. Choi, H.-G., Son, M. & Choi, H. Integrating seawater desalination and wastewater reclamation forward osmosis process using thin-film composite mixed matrix membrane with functionalized carbon nanotube blended polyethersulfone support layer. *Chemosphere* **185**, 1181–1188 (2017).

54. Lu, P. et al. Layered double hydroxide/graphene oxide hybrid incorporated polysulfone substrate for thin-film nanocomposite forward osmosis membranes. *RSC Adv.* **6**, 56599–56609 (2016).

55. Liu, S., Fang, F., Wu, J. & Zhang, K. The anti-biofouling properties of thin-film composite nanofiltration membranes grafted with biogenic silver nanoparticles. *Desalination* **375**, 121–128 (2015).

56. Tian, H., Wu, X. & Zhang, K. Polydopamine-assisted two-dimensional molybdenum disulfide (MoS2)-modified PES tight ultrafiltration mixed-matrix membranes: enhanced dye separation performance. *Membranes* **11**, 96 (2021).

57. Wu, X., Fang, F. & Zhang, K. Graphene oxide modified forward osmosis membranes with improved hydrophilicity and desalination performance. *Desalin. Water Treat.* **85**, 73–83 (2017).

58. Park, M. J. et al. Graphene oxide incorporated polysulfone substrate for the fabrication of flat-sheet thin-film composite forward osmosis membranes. *J. Membr. Sci.* **493**, 496–507 (2015).

59. Emadzadeh, D., Lau, W. J., Matsuura, T., Rahbari-Sisakht, M. & Ismail, A. F. A novel thin film composite forward osmosis membrane prepared from PSf–TiO2 nanocomposite substrate for water desalination. *Chem. Eng. J.* **237**, 70–80 (2014).

60. Loeb, S., Titelman, L., Korngold, E. & Freiman, J. Effect of porous support fabric on osmosis through a Loeb–Sourirajan type asymmetric membrane. *J. Membr. Sci.* **129**, 243–249 (1997).

61. Nguyen, T.-T., Lee, C., Field, R. W. & Kim, I. S. Insight into organic fouling behavior in polyamide thin-film composite forward osmosis membrane: critical flux and its impact on the economics of water reclamation. *J. Membr. Sci.* **606**, 118118 (2020).

62. Liu, Z. et al. Investigation of internal concentration polarization reduction in forward osmosis membrane using nano-CaCO3 particles as sacrificial component. *J. Membr. Sci.* **497**, 485–493 (2016).

## ACKNOWLEDGEMENTS

## AUTHOR CONTRIBUTIONS

X.W.: Conceptualization, investigation, methodology, validation, writing-original draft, writing-review and editing. F.F.: Investigation, methodology. B.Z.: Investigation, methodology, writing-review and editing. J.W.: Investigation, methodology, writing-review, and editing. K.Z.: Conceptualization, writing-review, and editing, funding acquisition, project administration.

## COMPETING INTERESTS

The authors declare no competing interests.

## ADDITIONAL INFORMATION